



SAKARYA ÜNİVERSİTESİ

FEN BİLİMLERİ ENSTİTÜSÜ DERGİSİ

Sakarya University Journal of Science
SAUJS

ISSN 1301-4048 e-ISSN 2147-835X Period Bimonthly Founded 1997 Publisher Sakarya University
<http://www.saujs.sakarya.edu.tr/>

Title: Robust Discrete-Time Hybrid Controller for Non-Inverting Buck-Boost DC-DC Converter

Authors: Faruk YALÇIN, İrfan YAZICI

Received: 2022-09-30 00:00:00

Accepted: 2022-11-28 00:00:00

Article Type: Research Article

Volume: 27

Issue: 1

Month: February

Year: 2023

Pages: 68-82

How to cite

Faruk YALÇIN, İrfan YAZICI; (2023), Robust Discrete-Time Hybrid Controller for Non-Inverting Buck-Boost DC-DC Converter. Sakarya University Journal of Science, 27(1), 68-82, DOI: 10.16984/saufenbilder.1182049

Access link

<https://dergipark.org.tr/en/pub/saufenbilder/issue/75859/1182049>

New submission to SAUJS

<http://dergipark.gov.tr/journal/1115/submission/start>

Robust Discrete-Time Hybrid Controller for Non-Inverting Buck-Boost DC-DC Converter

Faruk YALÇIN^{*1} , İrfan YAZICI² 

Abstract

This paper presents a robust hybrid controller for non-inverting buck-boost (NIBB) DC-DC converter. The proposed hybrid controller is comprised of feedback closed-loop PID controller and novel designed feedforward open-loop controller. The proposed open-loop controller supports the PID controller and enhances the system transient response during the system operating parameters transition. The open-loop controller has a simple and static structure. It is also independent of the closed-loop controller and thus has a modular behaviour. In order to show the accuracy, robustness and efficiency of the proposed hybrid control method, both simulation and experimental studies are performed. The comparative results prove that the proposed hybrid controller with the novel developed open-loop controller provides robust and efficient control of the converter. It improves the converter's output response during the transients of the operating parameters: the change of input voltage, reference output voltage and output load.

Keywords: Non-inverting, buck-boost converter, PID, open-loop controller

1. INTRODUCTION

Traditional buck-boost DC-DC converters are used widely in many areas such as adjustable power supplies, DC motor control, etc. where various direct voltage levels are required. So, there are many studies on these converters in the literature and the research about them still continues. In the conventional buck-boost converter topologies, output voltage polarity occurs

opposite of input voltage polarity [1-3]. Because of this, common-ground point cannot be obtained in these topologies. So, this circumstance increases the measurement difficulties and instrumentation cost of these converter applications.

The researchers study NIBB converter topologies in the literature in order to prevent reverse polarity and to overcome the related mentioned problems in the

* Corresponding author: farukyalcin@sakarya.edu.tr; farukyalcin@subu.edu.tr (F YALCIN)

¹Sakarya University of Applied Sciences, Faculty of Technology, Department of Mechatronic Engineering, Sakarya, Turkey.

ORCID: <https://orcid.org/0000-0003-2672-216X>

² Sakarya University, Faculty of Engineering, Department of Electrical-Electronics Engineering, Sakarya, Turkey.

E-Mail: iyazici@sakarya.edu.tr

ORCID: <https://orcid.org/0000-0003-3603-7051>



conventional ones. Both lower and higher output voltages than the input voltages can be obtained in the NIBB converters as well as the inverting converters [4, 5]. But, the output and the input voltage polarities are the same in the NIBB converters, and thus, a common-ground point between the input and the output can be achieved [6]. There are two main basic topologies for the NIBB converter. The first one is structured by two active switches and two diodes [7], whereas the second one is comprised of four active switches [8]. There are other many various developed converter topologies to enhance the converter operation [9, 10]. The converter studies where soft switching techniques are applied also exist in the literature [11, 12]. Although the main advantage of NIBB converters is obtaining positive output voltage, NIBB converters can also be transformed to only buck or only boost converter topologies if required, just through the proper control of the active switches of the NIBB converter circuit [13, 14].

In the literature, there are two main control methods for NIBB converters as well as the other DC-DC converters: voltage mode control [15, 16] and current mode control [17, 18]. For both of the mentioned two types of control, various closed-loop controllers are applied successfully for the control of NIBB converters. The conventional PI controller is applied for the control of the converter in many applications due to the simple structure of this controller [19-27]. The studies where the conventional PID controller is applied instead of the PI controller also exist to enhance the output response during the operating parameters change [28]. In some studies for the control of the converter, the well-known and frequently used compensators in control systems such as type-II [29] and type-III [30] ones are also preferred. Some researchers synthesize PI and PID controllers with various techniques for improvement of the converter control. Almasi et al. [31, 32] apply fuzzy PI control

to the converter successfully. Adaptive PI technique [33] and ant colony algorithm optimized PI control method [34] are also performed in the converter control in a successful manner. Celikovic et al. [35] perform a closed-loop control method combining PID control and Sliding Mode Control (SMC) to the converter. Other studies except these mentioned studies using other various closed-loop control methods such as model predictive control [36], adaptive on-time control [37] and backstepping control [38, 39] also exist in the literature.

Although various type control methods are used in the mentioned studies given in the previous paragraph, all of them are completely structured by closed-loop controllers. As it is well known, NIBB converters have nonlinear behavior like the other DC-DC converters. So, the closed-loop controllers for the NIBB converters need to be designed for a determined operating point through linearizing. Thus, it is clear that this causes the output response performance to get worse according to design criteria and the possibility of the system instability, when the converter is operated in different points from the determined operating point for the controller design. So, in order to improve the system performance and to reduce the instability possibility for any each operating point, various solutions where the closed-loop feedback control structures are supported by the open-loop feedforward control ones are developed and studied. In [40] and [41], open-loop feedforward controllers are developed to support the traditional PI controllers for the current mode control of the NIBB converters. In other current mode controlled NIBB converter study, closed-loop control structure comprised of PID and SMC controllers are supported by a developed open-loop feedforward control method [42]. The developed open-loop controllers for the current mode controlled converters in [40-42] are determined as static algebraic equations that derive the

inductor current depending on the converter topology parameters and the existing operating parameters. But, the equations of the open-loop controllers in the mentioned studies are derived only considering the continuous conduction mode (CCM) and ideal topology parameters of the converters. So, it is clear that open-loop controllers developed in the mentioned studies cannot satisfy the required enhancement on converter output responses in practical applications and in discontinuous conduction mode (DCM) operations. However, the output responses where the open-loop controllers are not included to the system are not demonstrated in these studies, so, the enhancement effects of the open-loop controllers are not given comparatively.

In this study, a new hybrid controller is developed for the NIBB converter as a voltage mode control. A new developed open-loop controller supports the closed-loop PID controller in the proposed hybrid controller. The proposed open-loop controller has a simple, static and algebraic structure that can be easily obtained as a one-equation. Thus, it supports the PID controller to lead the output voltage to reach the reference voltage in a fast manner. The proposed hybrid control method has superiorities and overcomes the drawbacks of the similar ones given in the previous paragraph as follows:

- The real equivalent circuit of the converter is considered for the design of the proposed open-loop controller that is part of the hybrid controller to provide more accurate results for real practical applications.
- Detailed dynamic analysis considering the real parasitic components of all the elements in the converter topology is performed for the closed-loop PID controller that is part of the hybrid controller to provide accurate response for real practical applications.

- The open-loop controller is designed for both CCM and DCM operation of the converter.
- The output response of the converter is obtained for both the proposed open-loop controller exist and not in the control of the converter. Thus, the effect of the proposed controller in the hybrid control is demonstrated comparatively.

Both simulation and experimental test studies are performed to prove the accuracy and the efficiency of the proposed control method. In these test studies, results for the control of the converter where the proposed open-loop controller exist and not are obtained and compared. The comparative results show that the proposed hybrid controller improves the output voltage response performance and enhances indirectly the system stability of the NIBB converter during the change of output reference voltage, input voltage, and output load.

2. THE NIBB CONVERTER

In this section, the topology of the NIBB converter studied in the paper and the operation procedure of the converter are given. Detailed dynamic analysis through the real equivalent circuit of the converter is obtained and converter design parameters are given.

chapter 2 title

2.1. The Topology

The NIBB converter topology studied in this study is given in Fig. 1. The topology is structured as well-known in the literature by two active switches and two diodes.

As shown in Fig. 1, the active switches S_1 and S_2 are selected as MOSFETs. D_1 and D_2 are the diodes. In Fig. 1, V_i , V_o , L , C , R , i_L , i_C and i_o represent the input voltage, the output voltage, the inductor, the capacitor, the ohmic load, the inductor current, the

capacitor current and the output current, respectively.

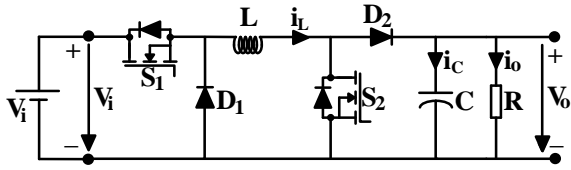


Figure 1 The NIBB converter topology

2.2. The Operation Procedure

In principle, the operation procedure of the NIBB converter is similar to the well-known traditional inverting buck-boost converter. Lower, equal and higher output voltages according to the input voltage can be obtained. S1 and S2 switches in Figure 1 are controlled simultaneously and in the same mode. So, the operation of the converter can be analyzed in two equivalent subcircuits in on-mode and off-mode. S1 and S2 switches are off together in the on-mode and together off in the off-mode. The converter subcircuits of both the on-mode and off-mode can be demonstrated in Fig. 2 and the converter operation can be detailed through the subcircuits.

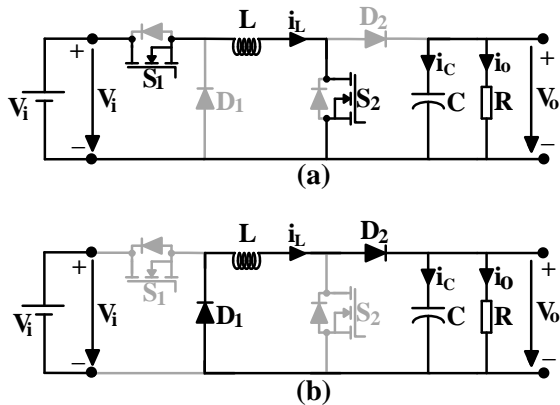


Figure 2 Converter subcircuits (a) on-mode subcircuit, (b) off-mode subcircuit

The on-mode subcircuit occurs when S1 and S2 switches are on during the on-time t_{on} of the switching period T_s as seen in Fig. 2a. During this mode, the diodes D1 and D2 become off due to S1 and S2 are on. Thus, the inductor L is energized by the input voltage and the inductor current i_L increases. Meanwhile, the pre-energized capacitor

supplies the load. The off-mode subcircuit occurs when S1 and S2 switches are off during the off-time t_{off} of the switching period as seen in Fig. 2b. During this mode, the diodes D1 and D2 become on due to the ongoing inductor current as S1 and S2 are off. Meanwhile, the pre-energized inductor supplies both the capacitor and the load. It is clear from the operation expressions, the main operation procedure is the same of the conventional inverting buck-boost converter. But as it is seen from Fig. 2, the output voltage polarity becomes the same of the input voltage, thus, a common-ground point can be obtained on the negative points of the input and the output. As a result, lower or higher output voltage according to the input voltage in the same polarity of the input can be produced by the NIBB converter through the proper control of the switching duty ratio d :

$$d = \frac{t_{on}}{T_s} \quad (1)$$

2.3. The Dynamic Analysis

The dynamic analysis of the converter is essential to design the control system of the converter. Both the closed-loop PID controller and the open-loop controller that are part of the proposed hybrid controller are designed through the mathematical model of the converter. Thus, the transfer function between the output voltage and the duty ratio for the PID controller design and the achievement of the static algebraic statement for the open-loop controller depend on the dynamic analysis. Providing the determined design criteria of the controllers for the real practical application depends on the dynamic analysis as possible as through the real equivalent circuit of the converter. For this aim, the real equivalent parasitic effects of the circuit elements are considered in the converter topology given in Fig. 1. So, the real equivalent model of the converter for the on-mode and the off-mode can be given through Fig.1 and Fig. 2 in Fig. 3.

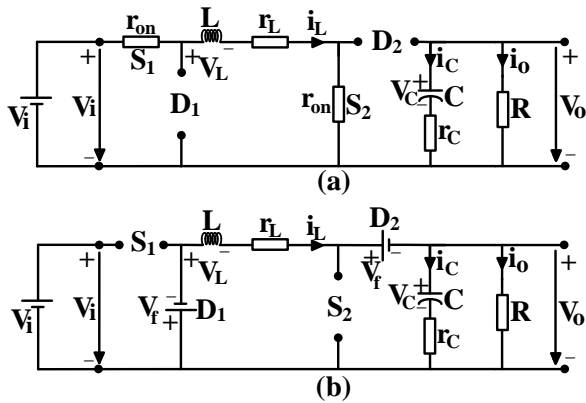


Figure 3 Real equivalent model of the converter (a) on-mode, (b) off-mode

In Fig. 3, r_{on} , r_L , r_C , V_f , V_L and V_C represent the on-resistance of MOSFET, equivalent series resistance (ESR) of the inductor, the ESR of the capacitor, forward biasing voltage of the diode, the inductor voltage and the capacitor voltage, respectively. In this study, the MOSFETs and the diodes are selected as identical.

The dynamic state equations of the state variables that are the inductor current and the output voltage for on-mode can be derived through Fig. 3a by using Kirchhoff's laws. The state equation of the inductor current for on-mode can be obtained by Fig. 3a as follows:

$$\frac{di_L(t)}{dt} = -\frac{1}{L}(r_L + 2r_{on})i_L(t) + \frac{1}{L}V_i \quad (2)$$

Similarly, the state equation of the output voltage for on-mode can be obtained by Fig. 3a as follows:

$$\frac{dV_o(t)}{dt} = -\frac{1}{(R+r_c)C}V_o(t) \quad (3)$$

The dynamic state equations of the state variables that are the inductor current and the output voltage for off-mode can be derived through Fig. 3b by using Kirchhoff's laws. The state equation of the inductor current for off-mode can be obtained by Fig. 3b as follows:

$$\frac{di_L(t)}{dt} = -\frac{r_L}{L}i_L(t) - \frac{1}{L}V_o(t) - \frac{2}{L}V_f \quad (4)$$

Similarly, the state equation of the output voltage for off-mode can be obtained by Fig. 3b as follows:

$$\begin{aligned} \frac{dV_o(t)}{dt} = & \frac{R}{R+r_c} \left[\frac{1}{C} - \frac{r_c r_L}{L} \right] i_L(t) \\ & - \frac{R}{R+r_c} \left[\frac{r_c}{L} + \frac{1}{RC} \right] V_o(t) - \frac{2r_c V_f R}{(R+r_c)L} \end{aligned} \quad (5)$$

The on-mode state-space model of the converter can be obtained from (2) and (3) as follows:

$$\begin{aligned} \begin{bmatrix} \dot{i}_L(t) \\ \dot{V}_o(t) \end{bmatrix} = & \begin{bmatrix} -\frac{1}{L}(r_L + r_{on}) & 0 \\ 0 & -\frac{1}{(R+r_c)C} \end{bmatrix} \begin{bmatrix} i_L(t) \\ V_o(t) \end{bmatrix} \\ & + \begin{bmatrix} \frac{1}{L} & 0 \\ 0 & 0 \end{bmatrix} \begin{bmatrix} V_i \\ V_f \end{bmatrix} \end{aligned} \quad (6)$$

By the similar way, the off-mode state-space model of the converter can be derived from (4) and (5) as follows:

$$\begin{aligned} \begin{bmatrix} \dot{i}_L(t) \\ \dot{V}_o(t) \end{bmatrix} = & \begin{bmatrix} -\frac{r_L}{L} & -\frac{1}{L} \\ \frac{R}{R+r_c} \left[\frac{1}{C} - \frac{r_c r_L}{L} \right] & -\frac{R}{R+r_c} \left[\frac{r_c}{L} + \frac{1}{RC} \right] \end{bmatrix} \begin{bmatrix} i_L(t) \\ V_o(t) \end{bmatrix} \\ & + \begin{bmatrix} 0 & -\frac{1}{L} \\ 0 & -\frac{r_c R}{(R+r_c)L} \end{bmatrix} \begin{bmatrix} V_i \\ V_f \end{bmatrix} \end{aligned} \quad (7)$$

Thus, the linearized small-signal transfer function of the converter between the output voltage and the duty ratio is derived from the state-space models given by (6) and (7) as below:

$$G_C(s) = \frac{\hat{V}_o(s)}{\hat{d}(s)} = \frac{gs + (ag + cf)}{s^2 + (a + e)s + (ae - bc)} \quad (8)$$

The coefficients a, b, c, e, f and g in (8) are given as follows:

$$a = \frac{(r_L + 2\bar{D}r_{on})}{L} \quad (9)$$

$$b = \frac{-(1-\bar{D})}{L} \quad (10)$$

$$c = \frac{(1-\bar{D})R}{R+r_c} \left[\frac{1}{C} - \frac{r_c r_L}{L} \right] \quad (11)$$

$$e = \frac{(1-\bar{D})Rr_c}{(R+r_c)L} + \frac{1}{(R+r_c)C} \quad (12)$$

$$f = \frac{-2r_{on}\bar{i}_L + \bar{V}_o + \bar{V}_i + 2V_f}{L} \quad (13)$$

$$g = \frac{R}{R+r_c} \left[-\left(\frac{1}{C} - \frac{r_c r_L}{L} \right) + \frac{r_c \bar{V}_o}{L} + \frac{2r_c R V_f}{L} \right] \quad (14)$$

In (9)-(14), \bar{D} , \bar{i}_L , \bar{V}_i and \bar{V}_o represent the duty ratio, the average inductor current, the input voltage and the output voltage of the converter in the operating point, respectively. The average inductor current and the output voltage in the operating point are calculated as follows:

$$\bar{i}_L = \frac{\bar{D}\bar{V}_i - 2(1-\bar{D})V_f}{(1-\bar{D})^2 R} \quad (15)$$

$$\bar{V}_o = \frac{\bar{D}\bar{V}_i - 2(1-\bar{D})V_f}{(1-\bar{D})} \quad (16)$$

2.4. The Design Criteria

The switching frequency f_s is determined with the selected inductor and the capacitor values depending on the analysis of the

converter time constant through the dynamic analysis given in section 2.3. The determined and measured values of the mentioned parameters are given in Table 1.

Table 1 The determined switching frequency, capacitance and inductance parameters for the converter circuit

Switching Frequency f_s (kHz)	Capacitor		Inductor	
	C (μ F)	r_c (m Ω)	L (μ H)	r_L (m Ω)
25	140.5	225	103.5	147

For the experimental study, n-channel IRFP250N ($V_{DSS}=200V$, $r_{on}=75m\Omega$, $I_D=30A$) is used for the S_1 and S_2 MOSFETS. MUR1560 ($I_F=15A$, $V_F=1.5V$, $V_R=600V$) is used for the diodes. The operating point of the converter is considered as given in Table 2.

Table 2 The determined operating point parameters for the converter circuit

\bar{V}_i (V)	\bar{D}	\bar{V}_o (V)	\bar{R} (Ω)
10	0.5652	10	40

3. THE PROPOSED HYBRID CONTROLLER

This section presents the proposed hybrid controller and its design. The general control scheme of the converter operation can be given in Fig. 4.

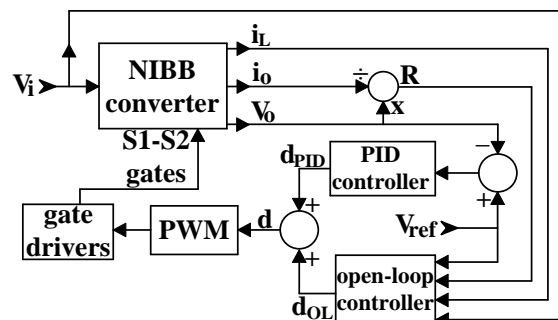


Figure 4 The general control scheme of the converter operation

In Fig. 4, V_{ref} determines the desired output voltage that can be lower, equal or higher according to the input voltage. As seen from Fig. 4, the closed-loop PID controller

provides the main control to obtain the output voltage through eliminating the error between the reference and the real output voltages. The proposed feedforward open-loop controller supports the closed-loop PID controller. The open-loop controller derives a static algebraic equation that aims to produce the duty ratio providing the desired output voltage. The duty ratio equation for the open-loop controller is obtained through the dynamic analysis of the converter for both CCM and DCM separately. Although the dynamic analysis is done for the real equivalent circuit of the converter, the duty ratio achieved by the open-loop controller cannot provide obtaining the desired real output voltage by oneself in real practical operation. Because in practice, the real values of the converter elements with the parasitic effects cannot be measured precisely. On the other hand, the parasitic inductance and capacitance of the experimental board are not considered in the analysis. Also, the switching characteristics of the MOSFETs and the diodes are considered ideal in the analysis, but it is clear that it is not like that in practice. Even so, it is clear that the duty ratio of the open-loop controller is obtained so close to the real operating duty ratio of the desired output voltage in a fast manner during the operating parameters change. So, the static open-loop controller leads the dynamic PID controller to the desired duty ratio point immediately when the operating parameters are forced to be changed. Thus, the open-loop controller augments the PID controller performance for reference voltage tracing of the real output voltage. In this way, the real output voltage reaches the reference voltage in a fast manner. The oscillations are reduced and thus the stability is increased indirectly.

As a result, the proposed hybrid control system is comprised of the closed-loop PID controller and the newly designed open-loop controller, as seen from Fig. 5. Fig. 5 demonstrates that d that is the real desired duty ratio of the converter operation is

obtained by the sum of d_{PID} and d_{OL} that are the duty ratio values produced by the closed-loop PID controller and the proposed open-loop controller, respectively:

$$d = d_{PID} + d_{OL} \quad (17)$$

As mentioned before, the duty ratio of the open-loop controller is obtained through the dynamic analysis of the converter for both CCM and DCM operations and it can be given as follows:

$$d_{OL} = \begin{cases} d_{OL-CCM} = \frac{V_o + 2V_f}{V_i + V_o + 2V_f} & , \text{if } i_L = 0 \\ d_{OL-DCM} = \sqrt[3]{\frac{2V_o^2(V_o + 2V_f)L}{V_i^2(V_i + V_o + 2V_f)T_s R}} & , \text{if } i_L > 0 \end{cases} \quad (18)$$

The proposed hybrid controller is designed in discrete-time. So, both the open-loop controller and the PID controller are performed as discrete-time controllers in a microcontroller. The discrete-time control block diagram for the converter control can be represented in Fig. 5 through the given control scheme in Fig. 4.

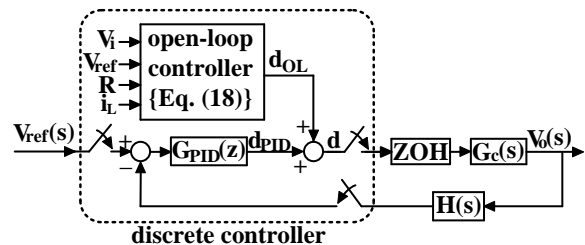


Figure 5 The discrete-time control block diagram of the converter

The static d_{OL} in (18) is performed at the each beginning of the switching period T_s . The discrete-time PID controller is designed through the closed-loop block diagram in Fig. 5. As seen from Fig. 5, d_{OL} affects the closed-loop system as a noise input. Thus, d_{OL} is considered as zero in the closed-loop PID controller design. Using the parameters given by Table 1 and 2 in (8), the continuous time transfer function of the converter is obtained as follows:

$$G_c(s) = \frac{2.422 \times 10^4 s + 7.049 \times 10^8}{s^2 + 3356s + 1.485 \times 10^7} \quad (19)$$

In Fig. 5, the transfer function of the measurement stage is $H(s)=1/10$. The ideal ADC transfer function and the microcontroller PWM stage transfer function are 1. The transfer function of the ZOH (zero order hold) is $(1 - e^{-sT_s})/s$. Thus, the discrete open-loop transfer function of the closed-loop control diagram except the PID controller can be derived as:

$$G(z) = Z \left\{ \frac{1 - e^{-sT_s}}{s} \cdot G_c(s) \cdot H(s) \cdot ADC(s) \cdot PWM(s) \right\} \quad (20)$$

$$= \frac{0.1441z - 0.0388}{z^2 - 1.852z + 0.8744}$$

In (20), $T_s=1/f_s=1/25\text{kHz}=40\mu\text{s}$. The transfer function of the discrete PID controller to be designed can be structured as:

$$G_{PID}(z) = K_P + K_I \frac{z}{z-1} + K_D \frac{z-1}{z} \quad (21)$$

The PID parameters in (21) are determined through the design in MATLAB-SISOTOOL environment by using (20) as below:

$$K_p = -1.9652 \times 10^{-4}, K_I = 0.0022, K_D = 1.26 \times 10^{-6} \quad (22)$$

The whole discrete open-loop transfer function of the converter system can be obtained using (20)-(22) as follows:

$$T(z) = G(z) \cdot G_{PID}(z)$$

$$= \frac{2.88 \times 10^{-4} z^3 - 4.96 \times 10^{-5} z^2 - 7.35 \times 10^{-6} z - 4.89 \times 10^{-8}}{z^4 - 2.852z^3 + 2.727z^2 - 0.8744z} \quad (23)$$

The Bode-diagram of the control block diagram in Fig. 5 is obtained in MATLAB through (23) in Fig. 6. It is clear from the Bode-diagram that the converter control system is stable with high gain margin(GM) and phase margin (PM).

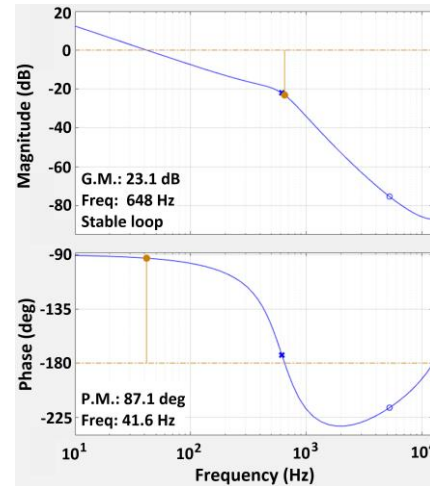


Figure 6 The Bode-diagram of the control block diagram

4. RESULTS

In this section, both simulation and experimental test studies are applied to the converter through the proposed hybrid control method. The simulation test studies are done in MATLAB-Simulink. A laboratory set-up is built for the experimental test studies as shown in Fig. 7.

Three different cases are determined for the test studies. The same test cases are applied to both the simulation and the experimental test studies to verify the theoretical and the practical accuracy. In these test cases, the operating parameters: reference output voltage, input voltage and the load are changed during the converter operation. Tracking the reference output voltage of the real output voltage is tested during the mentioned parameter changes for both the hybrid controller (PID + open-loop controller) and the only PID controller (where the open-loop controller does not exist). Thus, the accuracy and the efficiency of the proposed open-loop controller and hence the hybrid controller are proved comparatively.

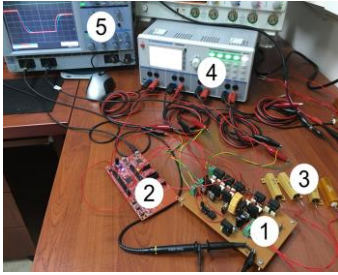


Figure 7 The laboratory setup: 1- NIBB converter circuit, 2- dsPIC33CH128MP508 based microcontroller card, 3- load, 4- power supply, 5- oscilloscope

Case-1 (reference voltage- V_{ref} change): In this case, the reference voltage is changed to different values when the input voltage and the output load are kept constant. The input voltage and the output load are in the operating points given in Table 2 ($V_i=10V$, $R=40\Omega$). The comparative output voltage waveforms for the reference voltage transients in the boost mode of the converter are given for simulation and experimental tests in Fig. 8 and Fig. 9, respectively.

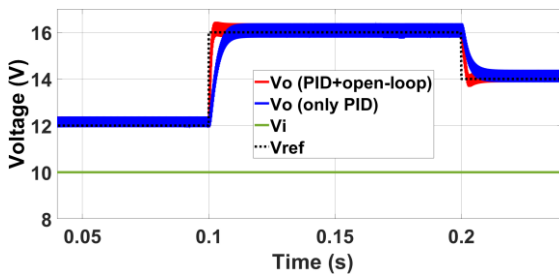


Figure 8 Simulation output voltage results for case-1 (boost mode – V_{ref} transients from 12V to 16V and from 16V to 14V)

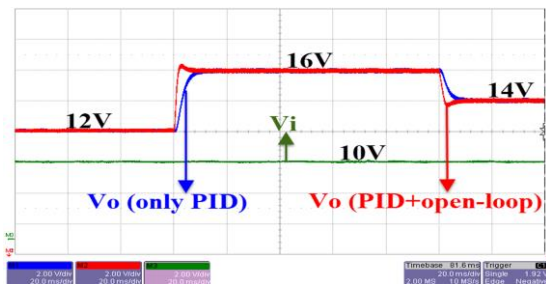


Figure 9 Experimental output voltage results for case-1 (boost mode – V_{ref} transients from 12V to 16V and from 16V to 14V)

A similar test study is performed for case-1 in the buck mode operation of the converter. The comparative output voltage waveforms for the reference voltage transients in the

buck mode of the converter are given for simulation and experimental tests in Fig. 10 and Fig. 11, respectively.

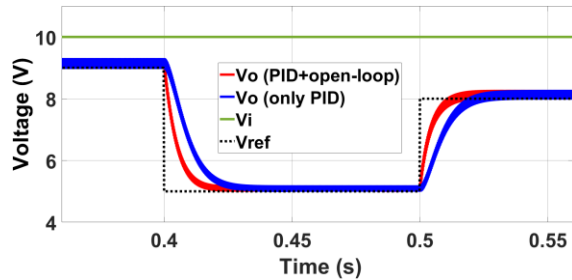


Figure 10 Simulation output voltage results for case-1 (buck mode – V_{ref} transients from 9V to 5V and from 5V to 8V)

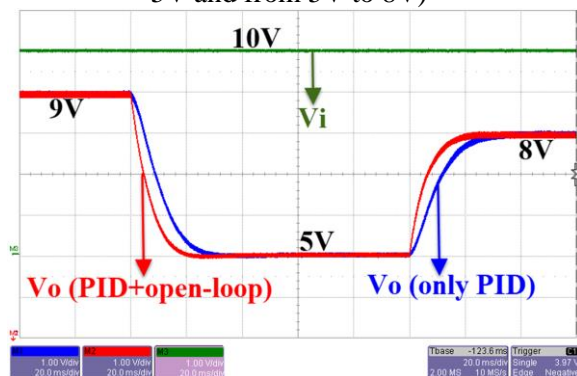


Figure 11 Experimental output voltage results for case-1 (buck mode – V_{ref} transients from 9V to 5V and from 5V to 8V)

The results for case-1 given in Fig. 8-11 show that the proposed hybrid controller provides the output voltage to reach the reference voltage in a fast manner during the reference voltage transients.

Case-2 (input voltage- V_i change): In this case, the input voltage is changed to different values when the reference voltage and the output load are kept constant. The reference voltage and the output load are in the operating points given in Table 2 ($V_{ref}=10V$, $R=40\Omega$). The comparative output voltage waveforms for the reference voltage transients in the boost mode of the converter are given for simulation and experimental tests in Fig. 12 and Fig. 13, respectively.

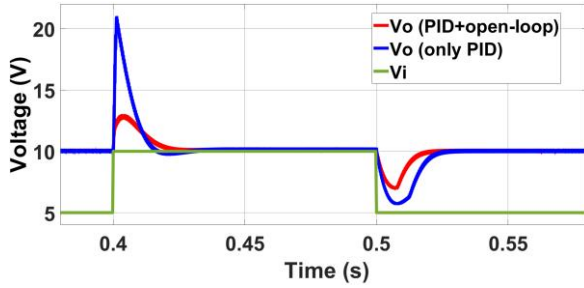


Figure 12 Simulation output voltage results for case-2 (boost mode – V_i transients from 5V to 10V and from 10V to 5V)

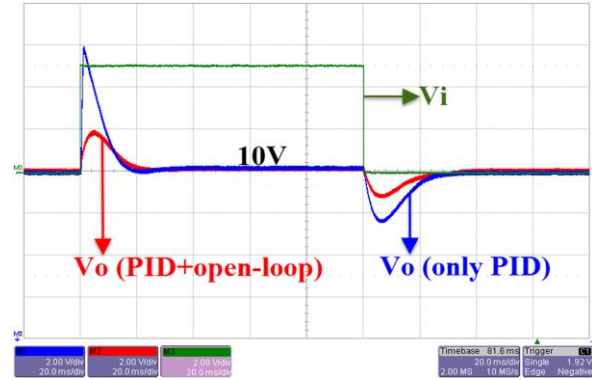


Figure 15 Experimental output voltage results for case-2 (buck mode – V_i transients from 10V to 15V and from 15V to 10V)

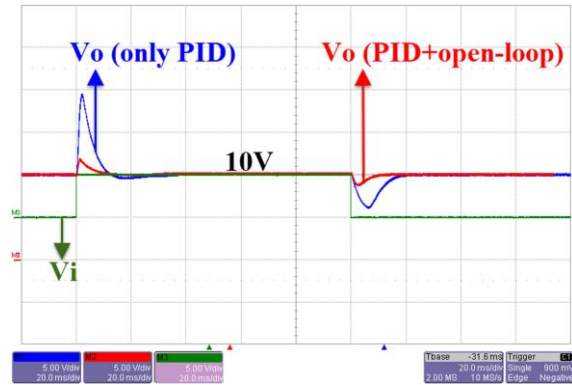


Figure 13 Experimental output voltage results for case-2 (boost mode – V_i transients from 5V to 10V and from 10V to 5V)

A similar test study is performed for case-2 in the buck mode operation of the converter. The comparative output voltage waveforms for the input voltage transients in the buck mode of the converter are given for simulation and experimental tests in Fig. 14 and Fig. 15, respectively.

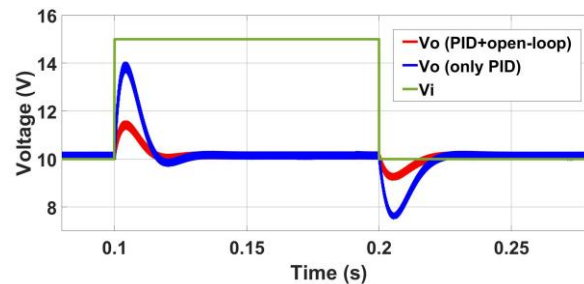


Figure 14 Simulation output voltage results for case-2 (buck mode – V_i transients from 10V to 15V and from 15V to 10V)

The results for case-2 given in Fig. 12-15 show that the proposed hybrid controller provides the output voltage to reach the reference voltage in a fast manner with also reduced oscillation during the input voltage transients.

Case-3 (output load-R change): In this case, the output load is changed to different values when the reference voltage and the input voltage are kept constant. The reference voltage and the input voltage are in the operating points given in Table 2 ($V_{ref}=10V$, $V_i=10V$). The comparative output voltage waveforms for the output load transients from 40Ω to 80Ω and again to 40Ω are given for simulation and experimental tests in Fig. 16 and Fig. 17, respectively.

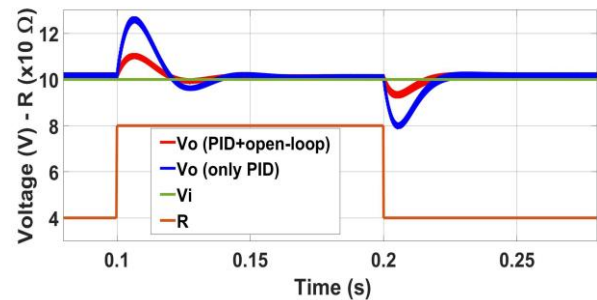


Figure 16 Simulation output voltage results for case-3 (R transients from 40Ω to 80Ω and from 80Ω to 40Ω)

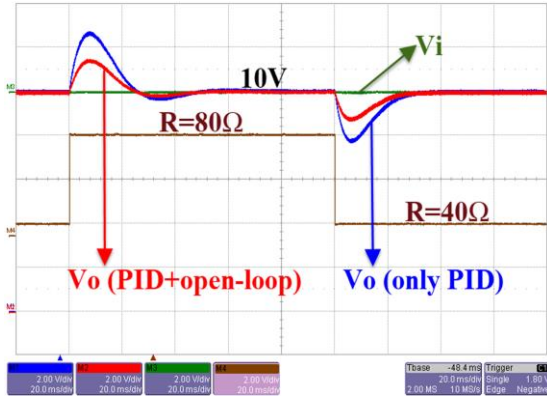


Figure 17 Experimental output voltage results for case-3 (R transients from 40Ω to 80Ω and from 80Ω to 40Ω)

A similar test study is performed for case-3 for the load transients from 40Ω to 30Ω and again to 40Ω. The comparative output voltage waveforms for the mentioned output load transients are given for simulation and experimental tests in Fig. 18 and Fig. 19, respectively.

The results for case-3 given in Fig. 16-19 show that the proposed hybrid controller provides the output voltage to reach the reference voltage in a fast manner with also reduced oscillation during the output load transients.

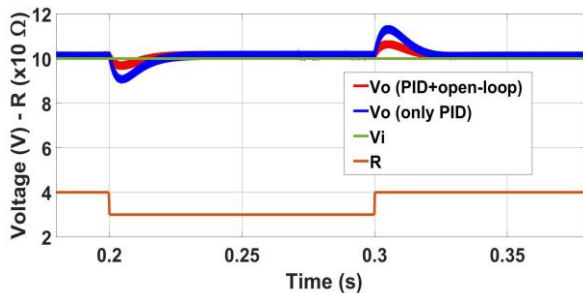


Figure 18 Simulation output voltage results for case-3 (R transients from 40Ω to 30Ω and from 30Ω to 40Ω)

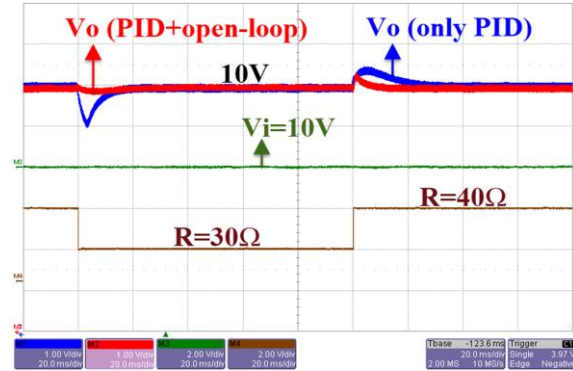


Figure 19 Experimental output voltage results for case-3 (R transients from 40Ω to 30Ω and from 30Ω to 40Ω)

The numerical comparison of the experimental results in terms of the overshoot (M_p %) and the settling time (t_{set} (ms)) are given in Table 3.

Table 3. The numerical comparison of the experimental results

Transient Case	M_p (%)		t_{set} (ms)	
	PID+ open-loop	PID	PID+ open-loop	PID
Case-1 (V_{ref})	12V→16V	0	2.2	22
	16V→14V	0	1.4	26
	9V→5V	0	0	26
	5V→8V	0	0	25
Case-2 (V_i)	5V→10V	20	95	16
	10V→5V	12	40	12
	10V→15V	18	59	30
	15V→10V	12	24	38
Case-3 (R)	40Ω→80Ω	15	28	50
	80Ω→40Ω	12	23	30
	40Ω→30Ω	3.1	20	20
	30Ω→40Ω	6	8	10

As result, both the simulation and experimental test studies for the given test cases show the theoretical and the experimental accuracy of the proposed hybrid controller for the NIBB converter control. Also, the test results prove that the proposed hybrid controller with the newly designed open-loop controller provides robust and efficient reference voltage tracking of the output voltage with improved performance during operating parameters change.

5. CONCLUSION

In this study, a new hybrid controller is designed for the NIBB converter. The developed open-loop controller supports the closed-loop PID controller in the proposed hybrid controller to enhance the output voltage response. The test results prove that the hybrid controller with the open-loop controller provides accurate, robust and efficient control of the converter. Thus, the output voltage tracks the reference voltage in a fast manner with reduced oscillation during the transients of the operating parameters such as reference voltage, input voltage and the output load. Independency of both the developed open-loop controller and the closed-loop PID that are part of the proposed hybrid controller provides modularity for the control system. Thus, any other closed-loop controller can be designed and included the hybrid controller instead of the PID controller without need of any change in the developed open-loop controller.

Funding

This study is supported as a scientific project by Sakarya University of Applied Sciences Scientific Research Projects Coordination Unit under grant no: 2021-01-04-033.

Authors' Contribution

The authors contributed equally to the study.

The Declaration of Conflict of Interest/ Common Interest

No conflict of interest or common interest has been declared by the authors.

The Declaration of Ethics Committee Approval

This study does not require ethics committee permission or any special permission.

The Declaration of Research and Publication Ethics

The authors of the paper declare that they comply with the scientific, ethical and quotation rules of SAUJS in all processes of

the paper and that they do not make any falsification on the data collected. In addition, they declare that Sakarya University Journal of Science and its editorial board have no responsibility for any ethical violations that may be encountered, and that this study has not been evaluated in any academic publication environment other than Sakarya University Journal of Science.

REFERENCES

- [1] C. Dong, W. Jiang, Z. Wang, F. Jiang, H. Jia, "Unified multimode modelling, stability analysis, and reinforced sliding-mode design of high-order buck/boost DC-DC converters for DC energy systems," *IET Energy Systems Integration*, vol. 3, no. 4, pp. 397-412, 2021.
- [2] M. Koundi, Z. El Idrissi, H. El Fadil, F. Z. Belhaj, A. Lassioui, K. Gaouzi, A. Rachid, F. Giri, "State-feedback control of interleaved buck-boost DC-DC power converter with continuous input current for fuel cell energy sources: theoretical design and experimental validation," *World Electric Vehicle Journal*, vol. 13, no. 7, article no. 124, 2022.
- [3] N. E. Zakzouk, A. K. Khamis, A. K. Abdelsalam, B. W. Williams, "Continuous-input continuous-output current buck-boost DC/DC converters for renewable energy applications: modelling and performance assessment," *Energies*, vol. 12, no. 11, article no. 2208, 2019.
- [4] A. L. Eshkevari, A. Mosallanejad, M. Sepasian, "Improving step-up gain and efficiency in non-inverting buck-boost dc-dc converter using quasi-Z impedance network," *IET Power Electronics*, vol. 15, no. 2, pp. 109-122, 2022.

- [5] G. Zhang, J. Yuan, S. S. Yu, N. Zhang, Y. Wang, Y. Zhang, "Advanced four-mode-modulation-based four-switch non-inverting buck-boost converter with extra operation zone," *IET Power Electronics*, vol. 13, no. 10, pp. 2049-2059, 2020.
- [6] X. Weng, X. Xiao, W. He, Y. Zhou, Y. Shen, W. Zhao, Z. Zhao, "Comprehensive comparison and analysis of non-inverting buck boost and conventional buck boost converters," *Journal of Engineering*, vol. 2019, no. 16, pp. 3030-3034, 2019.
- [7] O. Abdel-Rahim, A. Chub, A. Blinov, D. Vinnikov, "New high-gain non-inverting buck-boost converter," in *47th Annual Conference of the IEEE Industrial Electronics Society (IECON)*, Toronto, Canada, 2021.
- [8] A. Malou, B. Allard, A. Hijazi, X. Lin-Shi, "4-switch buck-boost DC-DC converter: a case study," *Journal of Low Power Electronics*, vol. 14, no. 4, pp. 558-571, 2018.
- [9] O. Abdel-Rahim, A. Chub, A. Blinov, D. Vinnikov, D. Pefititsis, "An efficient non-inverting buck-boost converter with improved step up/down ability," *Energies*, vol. 15, no. 13, article no. 4550, 2022.
- [10] H. Liao, J. F. Chen, "A two-phase non-inverting buck-boost converter for an RL load," *Journal of Engineering*, vol. 2022, no. 2, pp. 223-234, 2022.
- [11] Y. Zhang, X. F. Cheng, C. Yin, "A soft-switching non-inverting buck-boost converter with efficiency and performance improvement," *IEEE Transactions on Power Electronics*, vol. 34, no. 12, pp. 11526-11530, 2019.
- [12] X. F. Cheng, Y. Zhang, C. Yin, "A zero voltage switching topology for non-inverting buck-boost converter," *IEEE Transactions on Circuits and Systems-II: Express Briefs*, vol. 66, no. 9, pp. 1557-1561, 2019.
- [13] L. Cong, J. Liu, H. Lee, "A high-efficiency low-profile zero-voltage transition synchronous non-inverting buck-boost converter with auxiliary-component sharing," *IEEE Transactions on Circuits and Systems-I: Regular Papers*, vol. 66, no. 1, pp. 438-449, 2019.
- [14] M. Jabbari, S. Sharifi, G. Shahgholian, "Resonant CLL non-inverting buck-boost converter," *Journal of Power Electronics*, vol. 13, no. 1, pp. 1-8, 2013.
- [15] M. Fernandez, A. Rodriguez, M. Rodríguez, A. Vazquez, P. Fernandez, M. Arias, "Smooth-transition simple digital PWM modulator for four-switch buck-boost converters," *Electronics*, vol. 11, no. 1, article no. 100, 2022.
- [16] J. Moon, J. Lee, S. Kim, G. Ryu, J. P. Hong, J. Lee, H. Jin, J. Roh, "60-V non-inverting four-mode buck-boost converter with bootstrap sharing for non-switching power transistors," *IEEE Access*, vol. 8, pp. 208221-208231, 2020.
- [17] S. Lale, M. Soja, S. Lubura, D. D. Mancic, M. D. Radmanovic, "A non-inverting buck-boost converter with an adaptive dual current mode control," *Facta Universitatis-Series Electronics and Energetics*, vol. 30, no. 1, pp. 67-80, 2017.
- [18] H. Ramirez-Murillo, G. G. Huertas, C. A. Torres-Pinzon, J. E. Navarrete-Gomez, C. Restrepo, "LMI control design of a non-inverting buck-boost

- converter: a current regulation approach,” *Tecciencia*, vol. 12, no. 2, pp. 79-85, 2017.
- [19] B. N. Alajmi, M. I. Marei, I. Abdelsalam, N. A. Ahmed, “Multiphase interleaved converter based on cascaded non-inverting buck-boost converter,” *IEEE Access*, vol. 10, pp. 42497-42506, 2022.
- [20] T. Urkin, M. M. Peretz, “Digital CPM controller for a non-inverting buck-boost converter with unified hardware for steady-state and optimized transient conditions,” *IEEE Transactions on Power Electronics*, vol. 35, no. 8, pp. 8794-8804, 2020.
- [21] Z. Ortatepe, A. Karaarslan, “Pre-calculated duty cycle optimization method based on genetic algorithm implemented in DSP for a non-inverting buck-boost converter,” *Journal of Power Electronics*, vol. 20, no. 1, pp. 34-42, 2020.
- [22] B. Shi, Z. Zhao, K. Li, G. Feng, S. Ji, J. Zhou, “Design Methodology for Optimal Phase-Shift Modulation of Non-Inverting Buck-Boost Converters,” *Journal of Power Electronics*, vol. 19, no. 5, pp. 1108-1121, 2019.
- [23] M. Karimi, M. Pichan, A. Abrishamifar, M. Fazeli, “An improved integrated control modeling of a high-power density interleaved non-inverting buck-boost DC-DC converter,” *World Journal of Engineering*, vol. 15, no. 6, pp. 688-699, 2018.
- [24] A. H. M. Shalmaei, S. A. Gorji, “A non-inverting transformerless semi-quadratic buck-boost converter,” in *12th International Conference on Power, Energy and Electrical Engineering (CPEEE)*, Shiga, Japan, 2022, pp. 113-119.
- [25] J. Ma, M. Zhu, C. Pan, X. Cai, “Multimode operation of non-inverting buck boost converter for energy storage system,” in *IEEE 30th International Symposium on Industrial Electronics (ISIE)*, Kyoto, Japan, 2021.
- [26] F. Velasquez, A. Murthy, M. Badawy, “Simultaneous model based control of a non-inverting buck-boost converter for PFC applications at a reduced current stress,” in *IEEE Energy Conversion Congress and Exposition (ECCE)*, Baltimore, USA, 2019, pp. 1382-1388.
- [27] T. Urkin, M. M. Peretz, “Unified current-programmed digital controller for non-inverting buck-boost converter with optimal steady-state and transient conditions,” in *IEEE Applied Power Electronics Conference and Exposition (APEC)*, Anaheim, USA, 2019, pp. 199-206.
- [28] C. H. Tsai, Y. S. Tsai, H. C. Liu, “A stable mode-transition technique for a digitally controlled non-inverting buck-boost DC-DC converter,” *IEEE Transactions on Industrial Electronics*, vol. 62, no. 1, pp. 475-483, 2015.
- [29] J. S. Kim, J. O. Yoon, J. Lee, B. D. Choi, “High-efficiency peak-current-control non-inverting buck-boost converter using mode selection for single Ni-MH cell battery operation,” *Analog Integrated Circuits and Signal Processing*, vol. 89, no. 2, pp. 297-306, 2016.
- [30] J. K. Shiau, C. J. Cheng, “Design of a non-inverting synchronous buck-boost DC/DC power converter with moderate power level,” *Robotics and Computer-Integrated Manufacturing*, vol. 26, no. 3, pp. 263-267, 2010.
- [31] O. N. Almasi, V. Fereshtehpoor, M. H. Khooban, F. Blaabjerg, “Analysis,

- control and design of a non-inverting buck-boost converter: a bump-less two-level T–S fuzzy PI control,” *ISA Transactions*, vol. 67, pp. 515-527, 2017.
- [32] O. N. Almasi, V. Fereshtehpoor, A. Zargari, E. Banihashemi, “Design an optimal T-S fuzzy PI controller for a non-inverting buck-boost converter,” *Journal of Mathematics and Computer Science-JMCS*, vol. 11, no. 1, pp. 42-52, 2014.
- [33] A. Hajizadeh, A. H. Shahirinia, N. Namjoo, D. C. Yu, “Self-tuning indirect adaptive control of noninverting buck-boost converter,” *IET Power Electronics*, vol. 8, no. 11, pp. 2299-2306, 2015.
- [34] A. M. Bozorgi, V. Fereshtehpoor, M. Monfared, N. Namjoo, “Controller design using ant colony algorithm for a non-inverting buck-boost chopper based on a detailed average model,” *Electric Power Components and Systems*, vol. 43, no. 2, pp. 177-188, 2015.
- [35] J. Celikovic, A. Arguelloy, W. Alhoory, S. Abedinpoury, D. Maksimovic, “Sliding mode control with minimum-deviation transient response for non-inverting buck-boost DC-DC converters,” in *IEEE Applied Power Electronics Conference and Exposition (APEC)*, Phoenix, USA, 2021, pp. 482-486.
- [36] S. M. Ghamari, F. Khavari, H. Molaei, P. Wheeler, “Generalised model predictive controller design for a DC–DC non-inverting buck-boost converter optimised with a novel identification technique,” *IET Power Electronics*, early access, 2022.
- [37] Y. Y. Chen, Y. C. Chang, C. L. Wei, “Mixed-ripple adaptive on-time controlled non-inverting buck-boost DC-DC converter with adaptive-window-based mode selector,” *IEEE Transactions on Circuits and Systems II-Express Briefs*, vol. 69, no. 4, pp. 2196-2200, 2022.
- [38] O. Boutebba, S. Semcheddine, F. Krim, F. Corti, A. Reatti, F. Grasso, “A nonlinear back-stepping controller of DC-DC non inverting buck-boost converter for maximizing photovoltaic power extraction,” in *IEEE International Conference on Environment and Electrical Engineering and IEEE Industrial and Commercial Power Systems Europe (EEEIC / I&CPS Europe)*, Madrid, Spain, 2020.
- [39] K. S. Alharbi, R. A. McCann, “Non-overparametrized adaptive backstepping control of PWM DC-DC non-inverting buck-boost power converter,” in *IEEE Green Technologies Conference (GreenTech)*, Lafayette, USA, 2019.
- [40] V. I. Kumar, S. Kapat, “Digital hysteretic average current control for fast recovery in a non-inverting buck-boost converter,” in *IEEE Applied Power Electronics Conference and Exposition (APEC)*, Phoenix, USA, 2021, pp. 474-481.
- [41] V. I. Kumar, S. Kapat, “A digitally current mode controlled non-inverting buck-boost converter for fast voltage transitions,” in *IEEE Applied Power Electronics Conference and Exposition (APEC)*, Phoenix, USA, 2021, pp. 2520-2525.
- [42] Z. Chen, J. Hu, W. Gao, “Closed-loop analysis and control of a non-inverting buck–boost converter,” *International Journal of Control*, vol. 83, no. 11, pp. 2294-2307, 2010.